Biomechanics-Informed Mechatronics Design of Comfort-Centered Portable Hip Exoskeleton: Actuator, Wearable Interface, Controller

Daniel Rodríguez-Jorge⬤, Sainan Zhang⬤, Jin Sen Huang⬤, Ivan Lopez-Sanchez⬤, Nitin Srinivasan⬤, Qiang Zhang⬤, *Member, IEEE*, Xianlian Zhou⬤, *Member, IEEE*, and Hao Su⬤, *Senior Member, IEEE*

Abstract—Exoskeletons can improve human mobility, but discomfort remains a significant barrier to their widespread adoption. This paper presents a comfort-centered mechatronics design of portable hip exoskeletons, comprising of three factors: (i) actuation, (ii) wearable interface, (iii) and assistive controller. We introduced an analytical multibody model to predict the human-exoskeleton contact forces during gait. Informed by this model, we designed a wearable interface that significantly improved the three considered objective metrics: (i) undesired contact forces at the wearable interface, (ii) wobbling, and (iii) metabolic reduction, and also the post-test evaluation via a System Usability Scale questionnaire as a subjective metric. Our experiments with two exoskeleton controllers (gait-based and reinforcement learning-based) demonstrated that the design of the wearable physical interface has a greater impact on reducing metabolic rate and minimizing wobbling than the choice of controller. Our actuation design method leads to highly backdrivable, lightweight quasi-direct drive actuators with high torque tracking performance. By leveraging this wearable design, we achieved up to 60% reduction in undesired contact forces, and a 74% reduction in exoskeleton wobbling in the frontal axis compared to a traditional configuration. Additionally, the net metabolic cost reduction was 18% compared to the no exoskeleton condition.

Index Terms—Mechatronics design, hip exoskeleton, analytical multibody model, biomechanics, metabolic cost.

I. INTRODUCTION

EXOSKELETONS can assist human locomotion for both able-bodied individuals [1], [2], [3], and people with disabilities [4], [5]. Hip exoskeletons in particular can provide significant walking assistance [6], [7]. While state-of-the-art hip exoskeletons primarily focused on reducing metabolic cost during walking [8], [9], [10], user comfort when wearing an ankle exoskeleton was studied in [11]: comfort may also have a significant influence on the benefits in human performance the robot can deliver to the users. Reducing the metabolic cost of walking via a portable exoskeleton remains a significant challenge: different metrics of human performance may benefit to a greater or lesser extent from exoskeleton assistance. Objective metrics include muscle effort, joint power, and metabolic cost, for instance, while subjective metrics include user experience and usability. Although wearable robots can improve human performance [8], [9], [10], discomfort is one of their major limitations, still preventing their widespread adoption [12], [13]. Nevertheless, the metabolic rate reduction is typically chosen over comfort as a key objective metric to quantify robot performance. Hybart et al. [14] reported an 11% increase in metabolic cost with a portable ankle exoskeleton (Dephy, Inc.) versus the no-exo condition, applying an average peak torque of 17 Nm to the ankle joint. Contrastingly, other studies reported effective metabolic rate reduction using ankle exoskeletons, as in [15] (23% reduction in average), and [16] (11% reduction). These variations in findings highlight the complexity of optimizing exoskeleton designs and their impact on metabolic efficiency during walking. It remains unclear what is the appropriate level of assistive torque for the hip joint (Table I). A small assistance level of 6 Nm only led to a minor metabolic rate reduction of 7% [17], whereas a much larger assistance level of 140 Nm resulted in an increased metabolic rate, which may be due to the extra mass of the robot [18], alongside other design and control choices, such as the wearable interface between the robot and the human. On the other hand, solely focusing on metabolic rate reduction may lead to

Fig. 1. Our new proposed portable hip exoskeleton consists of two quasi-direct-drive actuators, adjustable width back frame, multi-strap wearable, and compact electronics. This design reduced wobbling (relative angular velocity between the human and robot) by 74% compared to a traditional configuration.

a biased design: the energetic benefit is not always perceivable to the users because the just-noticeable-difference in metabolic rate is about 22.7%, [19]. The wobbling of a robot (quantified by relative angular velocity between the human and robot) and subjective metrics such as user satisfaction via system usability survey (SUS) also play an important role in the multifaceted nature of human-robot interactions, comfort, and exoskeleton design, comprising actuation, wearable design, and control.

Underestimating the role of comfort in the mechatronics design of wearable robots has led state-of-the-art hip exoskeletons to often disregard their wearable design, namely using simple, single-strap configurations to secure the robot to the user's body [2], [20]. While this wearable configuration achieved some success in low-torque applications due to the lower contact forces and wobbling effects, it falls short in maintaining the stability and safety of the robot, especially under medium to high torque conditions: high contact forces at the human-exoskeleton interface may turn into a source of discomfort [21] and diminish the benefits of the robot. Thus, both actuation and also wearable design are key design choices that may impact the performance of wearable robots. Wearable design has been recently approached in the literature in an attempt to evaluate how it may impact exoskeleton performance. For instance, in [22] structured functional textiles are used in combination with a flexible actuation scheme to apply torque to the biological joints, highlighting the importance of assisting the user in a comfortable manner and concluding that reducing the pressure distribution is beneficial to reduce peak contact force. The maximum force applied to the human should be lower than the comfort limit at the point of application: in [21], the comfort limit for forces applied in different body segments/joints was characterized. A user-centered wearable interface for exoskeletons aimed at paraplegic users was introduced in [23], improving SUS and reducing pain for their target population. In [24], authors investigated various methods to enhance the wearing comfort

of exoskeleton robots, including mechanism design, and customized design of wearable structures. Excessive relative movement between the robot and the user may increase impact forces and decrease efficiency: in [25], simulated results showed that the impact force peaks increased with increasing rigid or wobbling masses of the lower body. In this paper, we demonstrate how wobbling also reduces the metabolic benefit of exoskeletons.

To address all the discussed design variables affecting discomfort in hip exoskeletons and enhance their benefits on users, we proposed a novel comfort-centered design for hip exoskeletons, which translates into the design of our three methods: (i) actuation, (ii) wearable configuration, (iii) and controller effect on exoskeleton performance. First, our actuation design method, after assessment of state-of-the-art actuators for wearable robots, aims at lower nominal torques for quasi-direct drive (QDD) actuators for hip flexion and extension, decreasing their weight while maintaining backdrivability. QDD actuation does not require springs or additional gears, improving efficiency. Second, our new wearable configuration (Fig. 1) enables a large range of motion and hip adjustability (Fig. 2), and departs from the single-strap configuration typically used in state-of-the-art exoskeletons (Fig. 4(a), top). By distributing the forces and torques across multiple attachment points, this approach seeks to enhance comfort and mitigate wobbling. In addition, the proposed wearable configuration does not noticeably increase the inertia of the robot, whose effect on the user's gait was proven to be significant for lower-limb exoskeletons [30]. This design is backed by a multibody model we developed that quantifies the human-exoskeleton contact forces at the straps during walking. Third, we evaluate the effects of two different controllers on our comfort metrics. In order to quantify comfort, we propose four different metrics: (i) contact forces experimented during the gait cycle at the wearable interface (straps), (ii) wobbling, and (iii) reduction in the metabolic cost of walking as objective metrics, and (iv) the SUS, which serves as a subjective measure of comfort.

The contributions of this work are as follows. (i) First, we introduced an actuation design method aiming at utilizing lower-nominal torque values tailored for walking with QDD actuators. This resulted in a lightweight, backdrivable hip exoskeleton (a bilateral weight of 3.71 kg with batteries compared to 4.2 kg of our previous design introduced in [31], and a unilateral weight of 2.9 kg) while maintaining high torque tracking performance. The actuator, with a norminal torque of 9 Nm and a peak torque of 18 Nm, is only 485 g. (ii) Second, we proposed an analytical, multibody model that estimates human-exoskeleton contact forces in the wearable interface (straps) during walking and informs the wearable design of a multi-strap, comfort-centered hip exoskeleton. Enhanced by this novel wearable configuration, our exoskeleton provides a significantly higher reduction in the energy cost of walking and reduces wobbling by around 74% in the frontal axis compared to a traditional configuration. (iii) Third, and although we do not introduce a new controller in this paper, in order to evaluate the factors that affect comfort, we quantified the effects of two existing controllers on metabolic cost and wobbling: a gait-based controller [31]

TABLE I

BENCHMARK OF STATE-OF-THE-ART PORTABLE HIP EXOSKELETONS. OUR EXOSKELETON ACHIEVES VERY SIGNIFICANT METABOLIC
REDUCTION AT A MEDIUM TORQUE LEVEL ASSISTANCE WITH THE LIGHTEST MOTORS

Exoskeleton	Metabolic rate reduction	Walking speed [m/s]	Assistive peak torque [Nm]	Actuator weight [kg]	Gear ratio	Total weight [kg]
This study	**-18.0%**	**0.9**	**9****	**0.485**	**9:1**	**3.44**[e]
Samsung [26]	-13.2%	1.14 ∼ 1.19	12	NA	50:1	2.6
Harvard[a] [6]	-9.3%	1.5	38.1	1.337	NA	4
Honda [17]	-7.1%[d]	1.06 ± 0.16	6	NA	NA	2.6
Utah [27]	NA	NA	41.9	0.567	2.5:1	2.5
Panasonic[b] [28]	NA	NA	10	0.58	16:1	9.3*
SSSA[c] [29]	NA	NA	10	1.2	80:1	4.2*

[a]Extension only; [b]Multiple DOFs; [c]Off-board electronics and batteries; [d]vs no assistance; [e]+270g battery; *With batteries; **Metabolic cost test using a peak torque of 9 Nm, while the actuator's peak torque is 18 Nm.

and a reinforcement-learning (RL)-based controller [32]. We also conducted a pilot test on one subject to quantify wobbling at two different walking speeds. Results showed that the choice of controllers did not have a significant effect on wobbling. The proposed actuation paradigm, along with wearable design informed by our human-exoskeleton contact force model, result in a lightweight, compliant, and high-torque hip exoskeleton that minimizes wobbling and improves human performance, achieving a higher metabolic rate reduction than the existing state-of-the-art robots, even at lower walking speeds.

II. DESIGN REQUIREMENTS OF PORTABLE EXOSKELETON

Hip exoskeletons have the potential to significantly reduce the metabolic cost of walking by assisting the hip joint, although some of their key design parameters comprising actuation, wearable design, and range of motion are often chosen heuristically, or without a model specifically designed to inform those choices, which may affect comfort.

Hip exoskeleton actuation design comprises the choice of unidirectional or bidirectional assistance, peak assistive torque, and the plane or planes of assistance. Hip exoskeletons may focus only on flexion (as in [33]) or extension (as in [34]) assistance, or actuate both [35]. Human-exoskeleton, computer-based simulations can be performed in order to determine optimal actuation profiles for either unidirectional or bidirectional assistance [36]. Those profiles can then be used to estimate the metabolic reduction caused by each profile and in consequence, choose the best actuation design. In addition, choosing the peak assistive torque in hip exoskeletons is a critical design factor: higher assistive torques tend to lead to higher metabolic reductions in ideal scenarios, but larger, heavier actuators and exoskeleton structure may hinder their performance. A 6 Nm peak torque only led to a minor metabolic rate reduction of 7% in [17], but largely increasing that peak torque to 140 Nm resulted in an increased metabolic rate due to the extra mass of the robot [18]. Hip exoskeletons that only provide unidirectional assistance [37] or excessive torque [18] may also result in inefficiencies that may hinder their metabolic rate reduction. Finding a balance between peak torque and mechanical design (total weight, mass placement, etc) is a key design challenge. Furthermore, abduction and adduction may also be considered as target degrees of freedom

for hip assistance. In [38], frontal assistance in hip exoskeletons did not show promising results in reducing the metabolic cost of walking, although a significant metabolic reduction with hip abduction assistance of up to 11.6% was observed in [39] with a tethered device.

In addition, wearable design is key in human-centered design of hip exoskeletons. Both the overall wearable configuration and the location of the contact interface between the human and the robot can affect how torque is transmitted, and thus, contact forces at the straps and possible wobbling. In our design, we aim at understanding how the wearable configuration can affect those undesired contact forces at the wearable interface, and propose a human-robot interface that minimizes such forces.

Finally, hip exoskeletons should provide an appropriate range of motion (ROM) and directions of assistance, as well as achieve enough level of assistive torque to enable agile tasks while still ensuring high compliance and kinematic stability, and not imposing restrictions on the user's motion in the frontal plane. Thus, our design approach and consequent exoskeleton provide active bidirectional assistance (extension and flexion) in the sagittal plane, while the frontal plane is unrestricted thanks to the use of passive hinges so that the user can perform abduction/adduction movements freely. The exoskeleton's hip joint should allow free movement in both sagittal and frontal planes. For typical level-ground walking, the human hip joint exhibits a range of motion encompassing 32.2° of flexion, 22.5° of extension, 7.9° of abduction, and 6.4° of adduction [31]. As for the overall device weight: a study was conducted in [40] to determine the effect of weight in hip exoskeletons, concluding that bilateral placement of a weight lower than 6 kg is more comfortable and transparent for the user, so we set a weight limit of 6 kg for the exoskeleton. Table II provides a summary of the design requirements, illustrating how our exoskeleton design effectively fulfills these criteria. With a total weight of 3.71 kg, lateral expandability of up to 15 cm (44 to 59 cm outer width), nominal velocity of 40 rad/s, and a peak torque output of 18 Nm, the exoskeleton can accommodate users of almost all waist sizes and deliver high torque while maintaining comfort, Fig. 2. To achieve that 44 to 59 cm lateral adjustability, we proposed a dual-arm design shown in detail in Fig. 1, which ensures structural rigidity with a thin cross-section and also facilitates the integration of a sliding mechanism: both aluminum bars that constitute our back frame
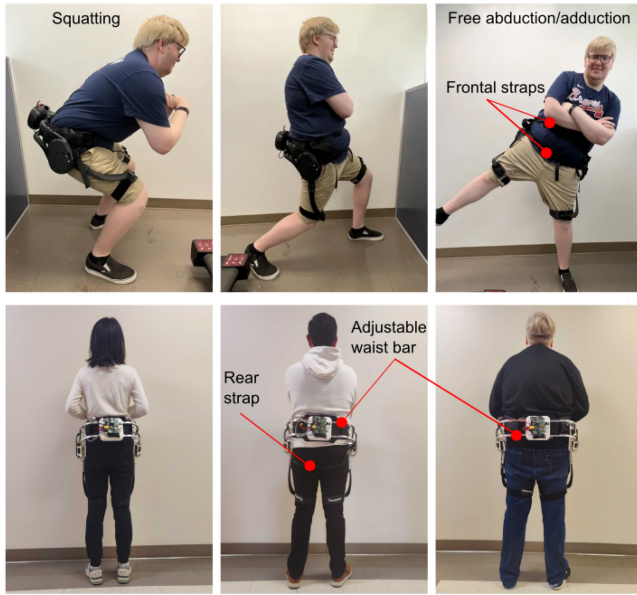
Fig. 2. Our portable hip exoskeleton enables a large range of motion for assisting versatile activities. The width of the back frame can also be extended to provide lateral adjustability to fit people with different waist sizes (one size for all).

TABLE II
DESIGN REQUIREMENTS AND SPECIFICATIONS

Parameters	Walking	Desired	Actual
Hip flexion/extension [º]	32.2/22.5	32.2/22.5	135/60
Hip abduction/adduction [º]	7.9/6.4	7.9/6.4	90/60
Flexion hip joint torque [Nm]	45	13.5	18
Max hip joint speed [rad/s]	2.3	3	40
Overall weight [kg]	-	6	3.71

are manufactured in two symmetric parts, the distance between which can be adjusted via a simple worm screw mechanism.

III. QUASI-DIRECT DRIVE ACTUATION

There are currently different actuation paradigms for powered exoskeletons, including Serial Elastic Actuators (SEA) [41], [42], pneumatic actuators [43], hydronic actuators [44], or quasi-direct drive actuation [3], [31], [45], [46], [47], which is one of the prevalent advances in actuation approaches for wearable robots. Quasi-direct drive actuators present reduced mass and size and are characterized by lower gear ratio and output inertia, the key to decreasing the resistance to human motion. Current actuators tend to improve backdrivability to the detriment of bandwidth, something particularly apparent in lower-limb exoskeletons. In our previous work [31], we designed a portable exoskeleton, with quasi-direct drive actuators, low gear ratio (8:1), and high torque, but it was rather heavy and bulky. After a computational analysis to evaluate the effectiveness of hip assistance to human walking and predict optimal torque profiles, we found that medium-level, bidirectional hip assistance achieved the greatest metabolic rate reduction: Fig. 3(b) shows optimal torque profiles for hip assistance in flexion, extension, and both with a peak of 18 Nm. The optimal assistive profile for either the flexion or the extension case was assumed to take the form of a raise-peak-fall curve within the gait cycle,
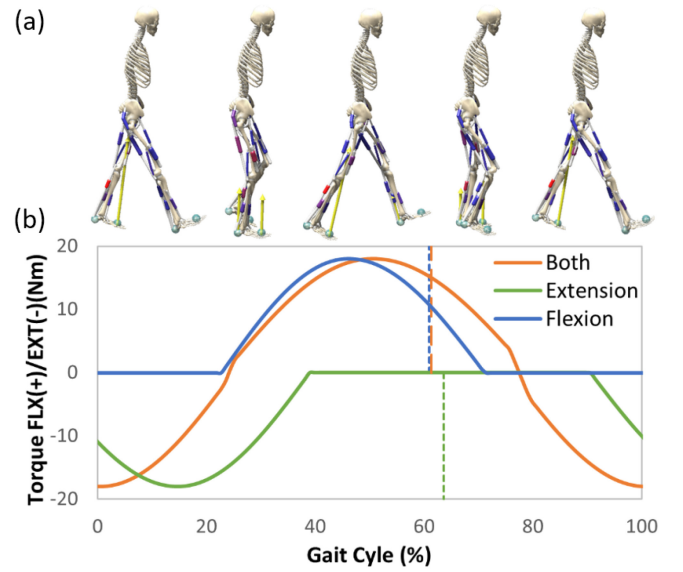

Fig. 3. (a) Computational biomechanics model for computing the optimal assistive profiles, represented along the gait cycle. (b) The predicted exoskeleton assistant torque profiles for flexion, extension, and both. Each vertical line indicates swing take-off time for the assistance of the corresponding color. The flexion and extension torque profiles are both predicted based on the start, rise, and fall time with a peak of 18 Nm [36]. The assistance with both flexion and extension is predicted by enabling both assistance during the optimization.

with parameters including the offset time, rise time, fall time, and peak torque. For cases where both flexion and extension assistance were provided, an interpolatory Catmull-Rom spline was used, parameterized by four time interval parameters. These parameters were optimized using the Covariance Matrix Adaptation Evolutionary Strategy (CMAES) method to minimize objective functions such as metabolic cost, [36]. The assistance profiles were optimized for normal walking of a subject with an approximate height of 1.8 meters and weight of 75.2 kg. Results show that bidirectional assistance is the most effective approach to reduce the metabolic cost of walking.

The torque generated by the motors must meet the design requirements: traditionally, the assessment of whether an exoskeleton meets the design requirements has been based solely on the actuator's peak torque being greater than the maximum required torque. However, this approach is insufficient without also considering the effective assistive torque, i.e., the root mean square (RMS) torque, generated by the controller over one cycle. For instance, for the torque profiles shown in Fig. 3(b), although all three have a peak torque of 18 Nm, their RMS torque values differ significantly, with the bidirectional configuration having higher RMS torque than the flexion-only and extension-only configurations. This implies that the bidirectional configuration imposes a higher demand on the actuator. Thus, it is essential to estimate the RMS torque produced by the controller over one cycle, which must be lower than or equal to the actuator's nominal torque. Second, the actuator's peak torque should be greater than the desired peak torque. The RMS torque in one gait cycle can be computed as:

$$\tau_{\text{RMS}} = \sqrt{\frac{\tau_1^2 + \tau_2^2 + \cdots + \tau_n^2}{n}} \tag{1}$$

where n refers to the subscript of the last assistive torque data in a gait cycle. Here we use one AK80-9 motor (Tmotor) with a 9:1 gear ratio per side resulting in a less bulky and lighter robot while maintaining the torque tracking and bandwidth performance of the device introduced in [31]. The AK80-9 motor has an 18 Nm peak torque and 9 Nm nominal torque at a 485 g mass, which represents a good balance between assistance and overall system weight. The motor has a built-in 14-bit resolution magnetic encoder. All metabolic rate tests were conducted with a peak torque of 9 Nm to ensure consistency in testing conditions, as one of the tested conditions (single-strap) exhibited excessive wobbling, which restricted the torque to a maximum of 9 Nm to ensure safety, whereas our wearable design exhibited much lower wobbling.

The frontal plane is left unactuated due to the drawbacks of translating frontal actuation to a fully portable device: the metabolic reduction found for a tethered device in [39] may be hindered by the extra complexity and added mass of the system.

IV. WEARABLE INTERFACE DESIGN AND MODELING

Although achieving the expected assistance requirements is the main goal when designing an exoskeleton for human assistance, it should not compromise user-centered features. Performance of hip exoskeletons can be hindered not only by discomfort or impracticability but also by efficiency losses caused by undesired vibrations and miss-alignments. In order to address these concerns, different conceptual configurations of hip-assistance exoskeletons were qualitatively reviewed. An analytical, multibody, human-exoskeleton interaction model for strap force analysis is also introduced, yielding predictions for the interaction forces and assessing the problem from a quantitative perspective and resulting in the proposed waist-based anchorage system. Finally, an expansion mechanism to improve adjustability among different users is presented.

A. Wearable Suit Design With Different Configurations

When considering high torque and agile activities, the distribution of forces plays a pivotal role in maintaining stability and user comfort. An exhaustive analysis of user comfort under forces applied to different body parts was performed in [21] in the context of human, wearable assistive robots. Forces were applied to a number of subjects, focusing on the shoulders, thigh, and shank, reaching two relevant conclusions: (i) shoulders showed the lowest maximum tolerable force, while the thigh showed the highest, and (ii) users saw their comfort limit increased over time due to habituation, yielding the maximum tolerance increase for the thigh, and the lowest for the shoulders. This suggests that shoulder straps may come with a comfort penalty for the user, making waist-only configurations more appealing. Fig. 4 (top) shows different conceptual designs for wearable configurations in a hip-assistance exoskeleton utilizing a single belt or with a lumbar support backpiece and shoulder straps. The optimal torque profiles in Fig. 3 obtained from the computational biomechanics model show high peak torque values appear in both flexion and extension phases for bidirectional actuation,
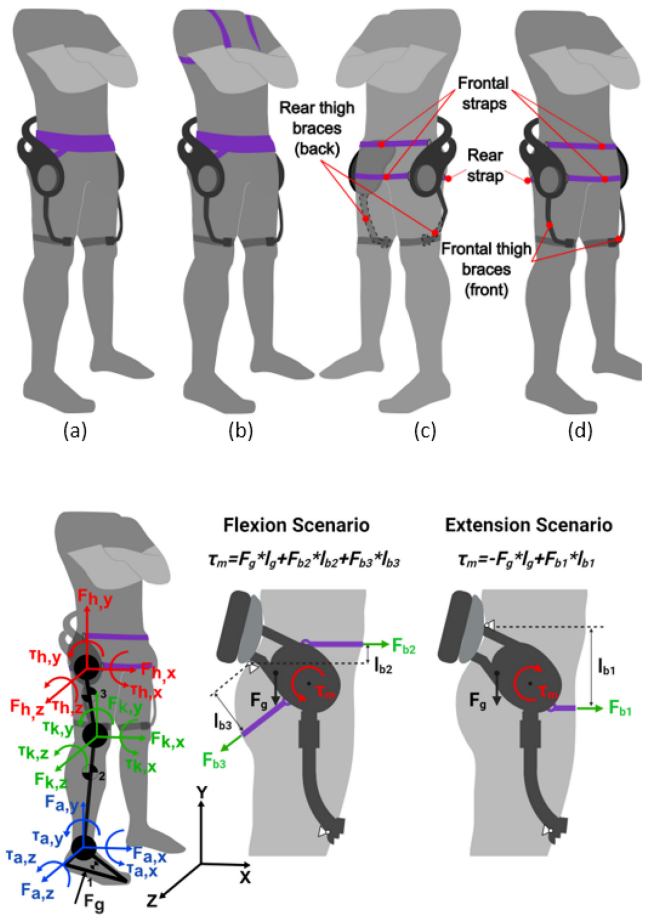

Fig. 4. Top: Four wearable design configurations for a portable hip exoskeleton, showcasing front thigh brace (a), (b), (d), and rear brace (c), as well as shoulder straps (b). (c, d) show a waist-based, multi-strap configuration. Shoulder straps (b) are commonly included to counteract the added weight and for high-torque applications. Results shown in this paper prevent including them, as the proposed approach reaches excellent performance without the additional comfort and wearability penalty. Computational analysis of bidirectional assistance torques, Fig. 3(b), suggests (c) or (d) are better solutions, of which (d) offer optimal wearability. Bottom: our analytical multibody model for the prediction of joint reaction torques and forces includes three segments of lower limbs (foot, shank, and thigh), the torso, and the exoskeleton. The robot produces a fraction of the total biological torque, from which total contact forces at the straps can be obtained. Joint reaction forces and torques were calculated from the ground reaction forces and kinematic data, while strap forces respond to equations (3) and (4).

suggesting either configuration (c) or (d) in Fig. 4 (top), of which (d) was chosen for our exoskeleton, since it makes it easier for the user to wear the robot without external help.

B. Analytical Multibody Model for Estimation of Human-Exoskeleton Interaction Forces and Torques

To minimize undesired rotations of the exoskeleton around the user's back when high torque is applied, our proposed design incorporates three waist belts that apply counter forces with substantial moment arms, illustrated in Fig. 4 (bottom). Two of these belts exert counterforces through tension when the exoskeleton's actuator plus the weight generate a counter-clockwise torque on the support (flexion assistance), while the third belt exerts counterforces against a clockwise torque from the exoskeleton (extension assistance).

When analyzing biological joint torques from a design perspective, 3D inverse-dynamics offer a reliable solution, especially when paired with accurate, kinematic data from a camera-based tracking system and force plates. As long as that information is available, joint torques and reaction forces can be easily predicted. Equation (2) yields the total hip reaction torques during unactuated gait in a fixed, inertial frame of reference from a given set of gait kinematics and the resulting joint forces and torques from the lower joints (knee and ankle):

$$\tau_{h,i} = I_{3,i}\dot{\omega}_{3,i} + \left(\omega_3 \times (I_3\omega_3)\right)\big|_i - \left(r_{gh}^h \times F_h\right)\big|_i + \cdots$$
$$\cdots + \left(r_{gh}^k \times F_k\right)\big|_i + n_{k,i} \tag{2}$$

where $\tau_{h,i}$ is the instantaneous joint torque at the hip, I_j stands for the inertia tensor of segment j, in this case the thigh (segment 3, the shank and the foot being segments 2 and 1 respectively, Fig. 4 (bottom)), ω_j would be the angular velocity of segment j, r_{gh}^h is a vector joining the thigh's center of mass (COM) with the hip joint and r_{gh}^k is the vector joining the thigh's COM with the knee joint. $F_{h,i}$ is the component i of the hip reaction force. In inverse dynamics, the total estimated joint torque at the hip is affected by the joint torques at the lower joints, knee, and ankle, in the form of the knee joint force $F_{k,i}$ and the knee joint torque $n_{k,i}$ (which are also affected by the ankle joint reactions).

Once the total biological torque is known from equation (2), the model shown in Fig. 4 (bottom) yields the resulting reaction forces applied by the exoskeleton upon the human body during operation via the straps during the flexion and extension phases, assuming kinematic invariance. Equations (3) and (4) yield the reaction forces at the waist during extension and flexion respectively, resulting from the combination of equation (2) and the model in Fig. 4 (bottom):

$$F_{b1} = \left(-\left(I_{3,i}\dot{\omega}_{3,i} + (\omega_3 \times (I_3\omega_3))\big|_i - (r_{gh}^h \times F_h)\big|_i + \cdots \right.$$
$$\left. \cdots + (r_{gh}^k \times F_k)\big|_i + n_{k,i}\right) \times C_h + F_g l_g\right)/l_{b1}, \tag{3}$$

$$F_{b3} \approx \frac{F_{b2}}{cos(\theta)} = \cdots$$
$$\cdots = \left(\left(I_{3,i}\dot{\omega}_{3,i} + (\omega_3 \times (I_3\omega_3))\big|_i - (r_{gh}^h \times F_h)\big|_i + \cdots \right.$$
$$\left. \cdots + (r_{gh}^k \times F_k)\big|_i + n_{k,i}\right) \times C_h - F_g l_g\right)/(l_{b2} \times cos(\theta) + l_{b3}), \tag{4}$$

where C_h is a constant determining the fraction of total hip torque to be assisted and θ is the angle between the rear strap and the vertical axis. Equation (4) assumes stationary state with near-zero horizontal acceleration. The support shown in Fig. 4 (bottom) only counteracts the exoskeleton's weight. For a single-strap configuration, equation (3) applies with the corresponding sign changes for flexion/extension. With a multi-strap configuration, equation (3) applies whenever motor torque provides extension assistance or $|C_h \times \tau_{h,i}| < |F_g l_g|$. If none of those conditions are satisfied, equation (3) must be used.

Reliable kinematic and ground contact force during gait are publicly available for multiple individuals in various databases [48], where several adults, both male and female, were tested on a treadmill and overground. Reaction forces
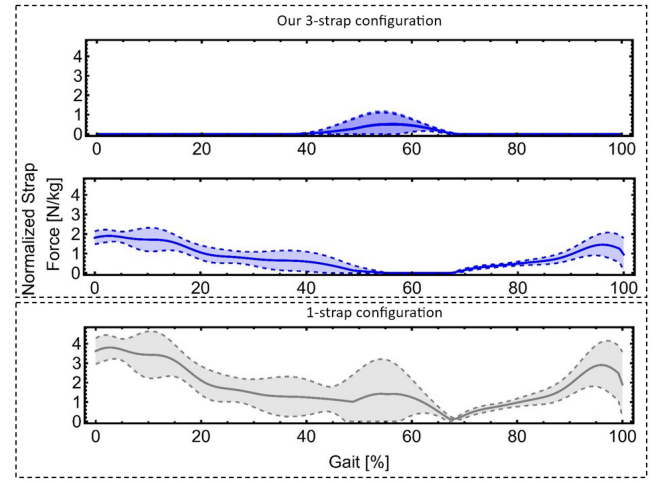

Fig. 5. Strap forces at the end of the stance and swing phase obtained from the analytical, multi-body model, F_{b2} and F_{b3} (blue, above) and at the stance phase F_{b1} (blue, below), for our multi-strap configuration, compared to a single-strap configuration (grey). Our proposed configuration reduces peak individual strap forces by 50% during hip extension and by 60% during flexion on average vs the single-strap configuration.

exerted by the exoskeleton upon the user in the waist area, the main contributor to vibrations and comfort, can then be easily estimated for different wearable configurations: subjects 27, 28, 31, and 33 in [48] were analyzed while walking overground at a comfortable speed. Anthropometric data for each subject is estimated following [49]. Kinematic data is filtered via a fourth-order low-pass Butterworth filter with a 10 Hz cut-off frequency with sample rates of 150 Hz. Sample rates of 300 Hz apply to dynamic data, including ground contact force magnitude and instantaneous center of pressure. Fixing an ideal actuation of 30% of the biological hip torque during gait results in the force evolution shown in Fig. 5.

When using the single-strap configuration, l_{b1} must be smaller than using our configuration, since the strap center of pressure must be located between both supports to remain stable during both flexion and extension assistance, which increases the strap force during extension. The proposed model can inform of the influence of design variables on the evolution of contact forces via parametric analysis. For instance, the geometric variables shown in Fig. 4 (bottom) can be analyzed within a certain range, which results in the following conclusions: (i) during the extension phases of gait, the maximum contact force at the single strap F_{b1} decreases the higher the distance l_{b1} is, albeit at a decreasing rate, and (ii) the maximum contact force during flexion decreases with l_{b2} but increases with l_{b3}.

C. Mechanism Design for Width Adjustability and Range of Motion

For rigid hip exoskeleton design, lateral adjustability is key to ensure usability in different users with distinct anthropometric characteristics. In response to this challenge, our exoskeleton offers an extensive lateral adjustability range, spanning from 44 cm to 59 cm in outer width, as opposed to many current exoskeletons, with limited or no adjustability.
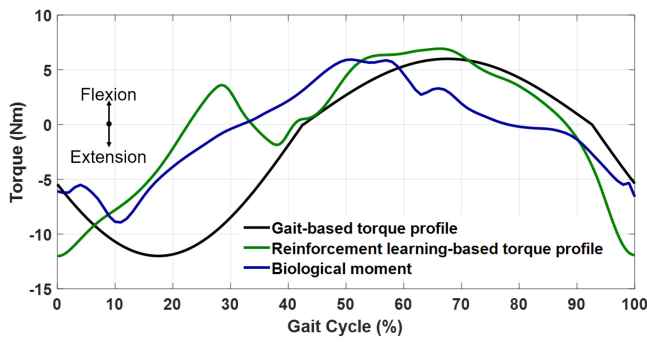
Fig. 6. Torque profiles with the gait-based controller (black) and reinforcement-learning-based (RL) controller (green), which were deployed on our hip exoskeleton to study their impact on wobbling and metabolic rate reduction at 1.25m/s. No significant difference in wobbling was observed between both controllers (Fig. 8(b)), but the RL-based controller showed a higher net metabolic cost reduction (Fig. 12(b)). In blue, scaled biological torque curve from [48].

This enhanced lateral adjustability is rooted in our dual-arm design, which not only fortifies structural rigidity but also facilitates the integration of sliding mechanisms with an extended range, accommodating individuals across a broad weight spectrum, ranging from 100 pounds to well over 300 pounds.

V. CONTROL AND ELECTRONICS OF OUR PORTABLE HIP EXOSKELETON

An important problem addressed in this study is determining which aspect—controller design or physical interface design—more effectively reduces wobbling and metabolic costs in exoskeleton users. To study the influence of different exoskeleton controllers on wobbling and metabolic cost, we chose two distinct controllers from our previous work: a gait-based controller [31] and a reinforcement-learning (RL)-based controller [32], [50]. The gait-based controller estimates the gait phase using the thigh angle and thigh angular velocity from one IMU sensor on each thigh. The estimated gait phase is then mapped to the assistance torque using a sine-shaped torque profile that is defined by five parameters: magnitude and duration of both extension and flexion assistance, and a constant shift. We tuned these parameters on each subject and the assistance profile from one representative subject is shown in Fig. 6. The RL-based controller also uses the thigh angle and angular velocity from the two thigh IMUs as the input to the exoskeleton control network. The output of the three-layer neural network is directly the assistance torque. We tuned the peak torque of this assistance profile on each subject and the assistance profile from one representative subject is shown in Fig. 6.

Our exoskeleton design is centered on portability, incorporating a detachable electronics module to assist mobility. We proposed a 3-layer portable mechatronics architecture. An onboard powerful computer (Raspberry Pi 4) establishes communication through a serial connection with the middle-level microcontroller (Cortex-M7 microcontroller, Teensy 4.1), receiving sensor data to generate the torque commands for the actuators. This high-speed microcontroller serves as the

central processing unit, managing communication between the onboard computer and the smart actuators. The low-level layer comprises lightweight smart actuators integrated with high-torque outer rotor BLDC motors and compliant gearboxes. The microcontroller utilizes the Controller Area Network (CAN) bus protocol as an interface with the smart actuators. For gait detection, two inertia measurement units (LPMS-B2 IMUs) were positioned in each thigh. For the power supply, an HRB lithium polymer battery (6 cells, 25.2 V, 270 g, 1.5 h battery life) is used to run the actuators.

VI. EXPERIMENTS AND RESULTS

The mechatronic design was experimentally tested to analyze how comfort is affected by the wearable design and control approach, which is achieved by quantifying three metrics in addition to contact forces: metabolic rate reduction in walking, wobbling (objective), and a SUS survey (subjective).

The experimental study involved four able-bodied subjects (28.5 ± 1.3 years old, 82.5 ± 21.7 Kg, and 175.3 ± 10.1 cm) for both metabolic cost and wobbling tests, who provided written informed consent to participate in the following experiment approved by the NC State University Institutional Review Board (IRB #26017). Four Inertial Measurement Units (IMUs) (LPMS-B2, LP-Research Inc., Japan) were used in the experiment. Two IMUs were attached to the left and right thighs to capture input for the controller, while the remaining two were used to measure wobbling—one mounted on the back of the exoskeleton (exo IMU) and the other on the participant's back (back IMU). Fig. 9 shows the IMU setup and both multi and single-strap wearable configurations. The RMS error between these two IMUs was used as a metric to quantify the wobbling of the exoskeleton, that is, its relative angular velocity concerning the human body in different conditions. Angular velocity data were filtered with a fourth-order Butterworth filter with a cutoff frequency of 20 Hz. Additionally, oxygen consumption was collected using portable respirometry equipment (VO2 analyzer, VO2 Master) for the assessment of energy expenditure. Experiments comprised four conditions: without exoskeleton (baseline), unpowered, power-on with one strap (state of the art), and power-on with one central strap and three auxiliary straps (proposed method). The third condition, power-on with one strap, is conducted with a traditional configuration with one unique central strap and without any auxiliary straps, all while using the same exoskeleton and controller: its main goal is comparing our proposed wearable configuration with one that resembles a more traditional design. A standing test was performed to compute the resting metabolic cost. The RL controller was used in all cases. When comparing different controllers, there were four randomized conditions: baseline, unpowered, powered with the gait-based controller, and powered with the RL controller. During each condition, participants were instructed to walk on a treadmill set at a constant speed of 0.9 m/s. Metabolic cost was collected throughout the 5-minute session, but only the last 2 minutes were analyzed. IMU data was collected for one minute, after
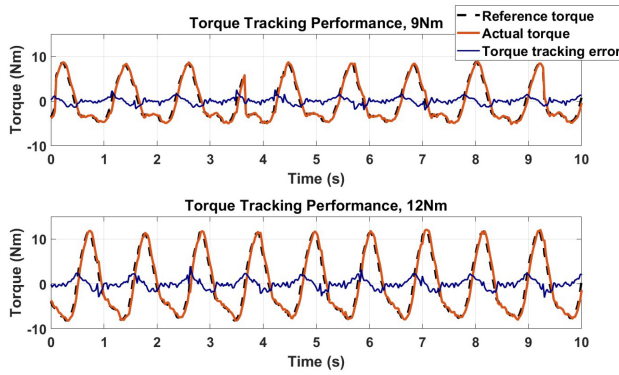
Fig. 7. Torque tracking performance of our exoskeleton for different peak torque values using the RL-based controller. Results were obtained during walking tests at 0.9 m/s. The mean of the applied assistive torque (red) showed an accurate torque tracking performance: 8.44% error for 9 Nm peak torque and 9.41% for 12 Nm. Relative torque error is shown in blue. In our tests, we restricted the peak torque to a maximum of 9 Nm to ensure safety in the single-strap configuration. To ensure consistency in testing conditions, all metabolic rate and wobbling tests were conducted with a peak torque of 9 Nm.

an initial delay of 30 seconds. An additional test was conducted with one subject walking at a higher speed of 1.2 m/s, measuring wobbling under both wearable configurations and controllers.

A. Evaluation of Torque Tracking of Portable Exoskeleton

A 29-year-old subject (80 kg) walked on a treadmill wearing the hip-assistance exoskeleton. Peak torques of 9 and 12 Nm were reached when walking. Fig. 7 shows the obtained torque profile with the proposed QDD device. The RMS error changed depending on the peak torque, as shown in Fig. 7: the average RMS error between the commanded torque and the measured torque was 0.76 Nm (8.44%) when providing 9 Nm peak torque and 1.13 Nm when providing 12 Nm (9.41%).

B. Wearable Design Effect on Wobbling and Metabolics

Our wearable design approach is intended to greatly improve comfort in hip assistance exoskeletons, which may also affect the metabolic cost reduction benefited by their users. Here, results obtained for both wobbling and metabolic costs for different wearable configurations are shown.

1) Effect of Wearable Design on Wobbling: Wobbling is directly affected by the wearable design. Fig. 8(a) shows the RMS between the user-fixed IMU and the robot-fixed IMU for angular speeds using our wearable configuration versus a traditional, single-belt configuration with a waist-only human-exoskeleton interface. The difference in angular velocity around the frontal axis (wobbling in the sagittal plane) between both IMUs increases when using the single-strap wearable configuration by 340.44% with respect to the unpowered case, but that increase is much lower at an average of 14.97% when using our configuration. Our wearable configuration reduces wobbling by an average of 73.90% with respect to the traditional configuration. Statistical significance was verified via one-sided paired t-tests, reaching p values of 0.277 and 0.004 between the powered case with our configuration and the
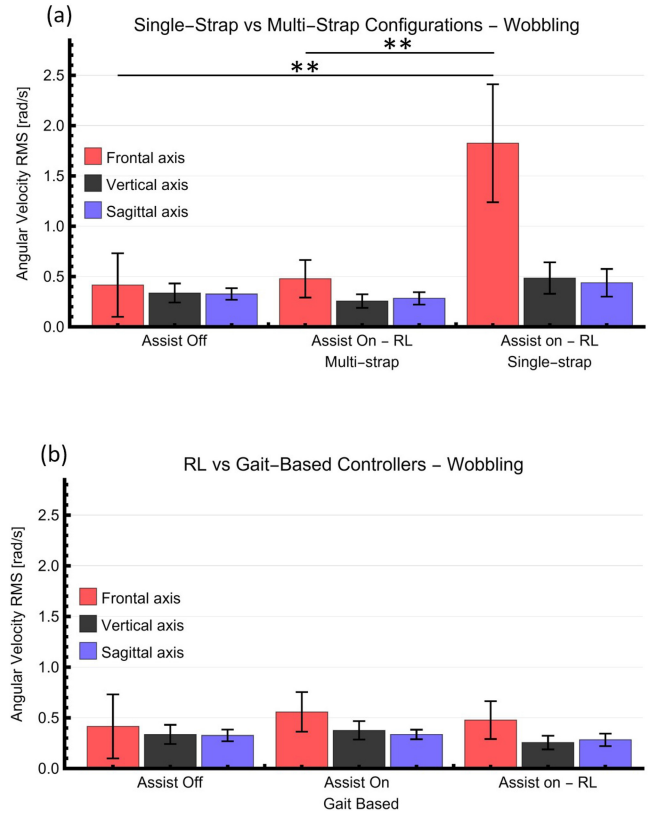

Fig. 8. (a) Wobbling reduction in the frontal axis: RMS and standard deviation (SD) for the relative angular velocity between the human and robot for the single-strap and our wearable configuration. Average frontal wobbling was reduced from 1.82 rad/s to 0.48 rad/s. (b) Wobbling for both the RL and gait-based controllers (with our wearable design). Both remain relatively close to the unpowered condition, which demonstrates our multi-strap wearable design can effectively improve comfort by reducing wobbling for different controllers. Statistical significance and p values were determined by one-sided paired t-test * $p \leq 0.05$, ** $p \leq 0.01$.

unpowered case, and between the single-strap configuration and the unpowered case, respectively. The p-value between the two wearable configurations was 0.005. Fig. 9 shows the relative angular velocity in the frontal plane measured for the two wearable configurations and the unpowered condition. In Fig. 5, results showed lower contact forces for the multi-strap configuration during gait, which may be related the lower wobbling values observed when using that configuration.

Walking speed may also affect wobbling. All experiments above were conducted at 0.9m/s. Fig. 10 shows the relative angular velocity RMS between the user and the subject for both controllers and wearable configurations for one subject walking at 0.9 and 1.2 m/s. The results show that higher speeds result in higher wobbling in all studied cases, as was expected: at 1.2 m/s, our configuration still reduced wobbling by 71.37% versus the single-strap configuration, although wobbling increased significantly compared to the 0.9 m/s speed.

2) Effect of Wearable Design on Metabolic Cost of Walking: Wobbling and misalignment resulting from the single-strap configuration can negatively affect the exoskeleton's performance and its impact on the user, even hindering their natural movement, yielding even increases in metabolic
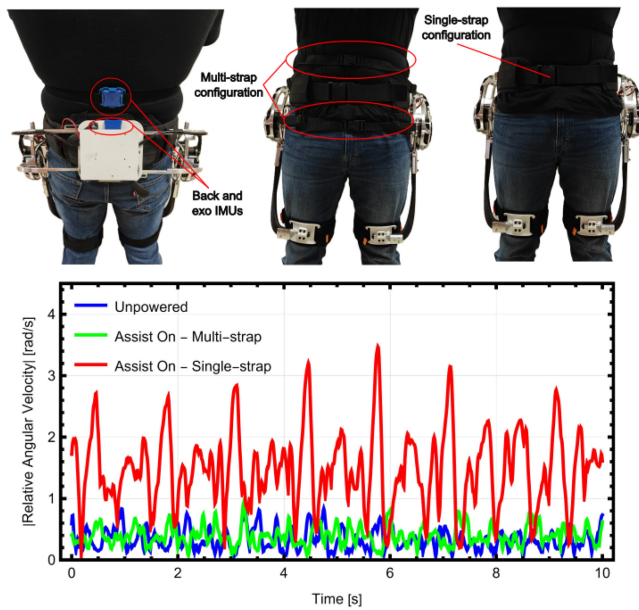
Fig. 9. IMU and wearable setup and time evolution of the measured frontal wobbling for the unpowered, single-strap, and multi-strap conditions. Under 1 m/s, our configuration maintains similar wobbling values to the unpowered case, whereas the single-strap configuration exhibits significantly higher average wobbling values, with the maximum exceeding 3 rad/s. This demonstrates that our multi-strap configuration can effectively improve comfort by reducing wobbling.
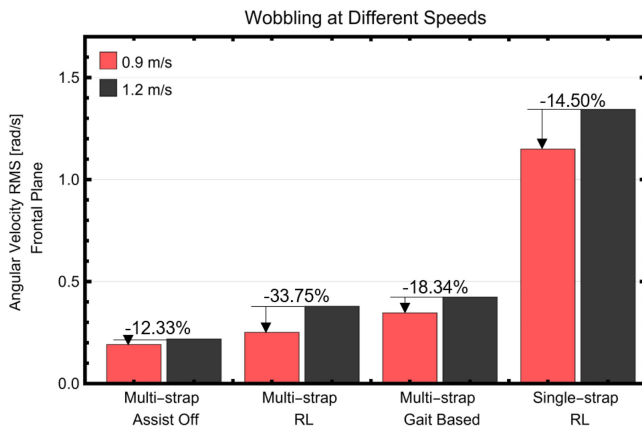

Fig. 10. Wobbling results in the frontal axis for two different walking speeds. Results at 1.2 m/s show an increase in frontal-plane wobbling in all conditions vs 0.9 m/s (33.3% increase in walking speed). Wobbling was 12.33%, 33.75%, 18.34%, and 14.50% lower at 0.9 m/s in the four cases, respectively: unpowered, with our wearable configuration and RL controller, same configuration with the gait-based controller, and with the 1 strap setup. Still, our multi-strap wearable configuration reduced most wobbling by 71.37% versus the single-strap configuration at 1.2 m/s.

cost. Fig. 12(a) shows how the two different wearable configurations affect the metabolic cost of walking in the experiments conducted following the described protocol. In order to avoid excessive wobbling when operating with the traditional, wearable configuration (see Fig. 8), peak torque values lower than the maximum, and of around 9 Nm, were used during the experiments. Using the RL controller, our wearable design achieves an 18% reduction in the metabolic cost of walking, while the single-strap configuration increases the metabolic
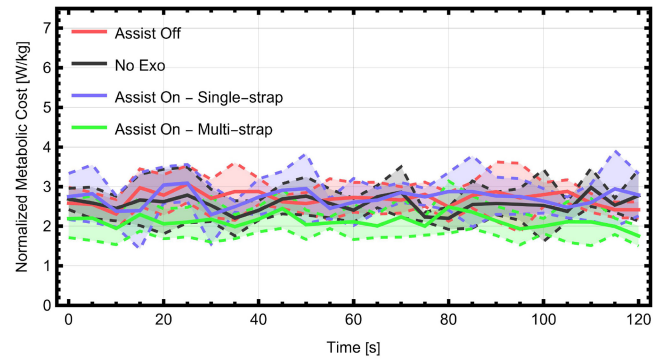
Fig. 11. Net metabolic cost during gait at 0.9 m/s measured in the last two minutes for all participants for both wearable configurations, without assistance and in the no exoskeleton condition, all using the RL-based controller. Average and standard deviation are shown for the tested population: the proposed configuration (green line) shows the lowest metabolic cost on average which had a reduction of 18% compared to wearing no exoskeleton. Fig. 12(a) shows the distribution of these results, average metabolic reductions, and statistical significance.

cost by 6.3% on average, both at around 9 Nm peak torque. Statistical significance was analyzed via one-sided paired t-tests, with p values of 0.009, 0.265, and 0.005 for the unpowered, single-strap, and multi-strap cases versus the baseline, respectively. A p-value of 0.014 was found between both wearable configurations. Fig. 11 shows the net metabolic cost of walking measured during the last two minutes for all subjects. The RL-based controller was also used in [50] on a different device and at a higher peak torque on 8 subjects walking at 1.25 m/s, reporting a metabolic reduction of 24.3%. Here, 18% reduction is achieved (Fig. 12) across 4 subjects at a lower peak torque of 9 Nm with the exoskeleton shown in Fig. 1.

C. Control Strategy Effect on Wobbling and Metabolics

In this section, experimental results are shown for relative angular velocity between the exoskeleton and the user under two distinct controllers described in Section V: an RL and a gait-based controller. Results obtained for wobbling and metabolic cost reduction are shown with our wearable configuration for both controllers.

1) Effect of the Controller on Wobbling: Computing wobbling by measuring the relative angular velocity between the robot and the user via IMUs results in Fig. 8(b), showing the RMS between both relative angular speeds using both proposed controllers. The difference in angular velocity in the 3 axes between both IMUs did not reach significant values when comparing both controllers, both remaining relatively close to unpowered values, albeit showing a slight decrease in the vertical and sagittal axes in the RL case, while the opposite happened in the frontal axis. None of the obtained results were found significant after the t-test. A similar conclusion is reached when comparing the effect of the controller on wobbling at different speeds. As in Fig. 10, wobbling with our proposed configuration is significantly lower than with the traditional single-strap, for both speeds, 0.9 and 1.2 m/s. For the tested subject, wobbling was more noticeable using the gait-based controller than the reinforcement learning controller
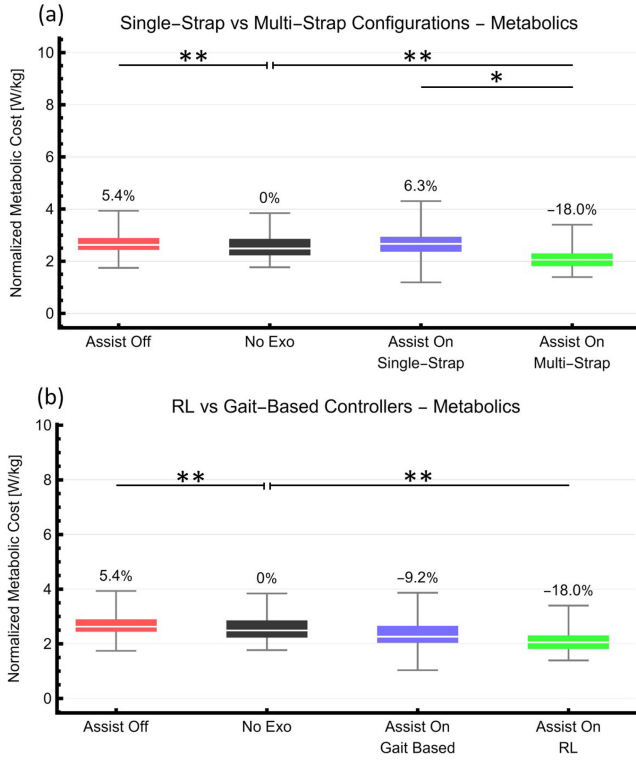
Fig. 12. (a) Our wearable configuration with RL-based controller resulted in a larger net metabolic rate reduction compared with the single-strap configuration, which did not allow more than 9 Nm torque due to excessive wobbling, illustrated in Fig. 8(a) (18% reduction versus a 6.3% increase, with the same 9 Nm peak torque). (b) Metabolic cost reduction result using RL-based controller vs gait-based controllers and in all cases with our multi-strap wearable configuration. RL achieves higher net metabolic rate reduction (18% vs 9.2%) at the same 9 Nm peak torque. Statistical significance and p values were determined by one-sided paired t-test, * $p \leq 0.05$, ** $p \leq 0.01$.

at both speeds: 37.73% higher at 0.9 m/s and 11.75% higher at 1.2 m/s.

2) Effect of the Controller on Metabolic Cost of Walking: The controller can also impact the metabolic cost of walking. Fig. 12(b) shows the metabolic cost reduction experimented by the tested population when using the proposed multi-strap configuration under the two described controllers. Metabolic differed between both: reinforcement learning yielded notably higher values for the metabolic cost reduction, showing an 18% reduction versus the no-exo condition, for the 9.2% reduction of the gait-based controller at the same peak torque of 9 Nm. The one-sided paired t-test yielded *p* values of 0.009, 0.064, and 0.005 for the unpowered, gait-based, and RL cases versus the baseline, respectively. A *p*-value of 0.109 was found between both controllers. Table III shows the individual metabolic results obtained for each participant.

D. Comfort Evaluation via SUS Survey

After the experiment session, participants provided feedback on the exoskeleton, yielding positive results for its usability and comfort during testing when using the proposed wearable configuration. For wearable robots to gain widespread acceptance, their comfort and usability for everyday activities are critical factors, as affirmed by the participants. The SUS is the

TABLE III
INDIVIDUAL EXPERIMENTAL RESULTS FOR METABOLIC RATE
REDUCTION VERSUS THE NO-EXO CONDITION

Subject	1	2	3	4
Weight [kg]	75	85	56	109
Height [cm]	180	181	160	180
Unpowered	+8.67%	+2.49%	+6.11%	+4.51%
Multi-strap RL	-11.17%	-16.03%	-26.36%	-17.26%
Single-strap RL	+32.30%	-0.87%	-2.29%	-3.82%
Gait based	-15.53%	+3.07%	-10.15%	-14.28%

most frequently used questionnaire to measure usability [51]. Our exoskeleton garnered a SUS score of 74, surpassing the average score of 68 (center of the Sauro-Lewis curved grading scale) [52]. The participants find the exoskeleton to be gentle on their skin and clothing, devoid of any irritations, abrasions, or wear and tear. Its ease of donning and secure fit, coupled with a manageable weight, further contribute to a positive user experience [53].

E. Discussion

This section presents the experimental results for metabolic reduction and wobbling with two different wearable configurations and two different controllers, in addition to the unpowered and no exo conditions and torque tracking results. These results show how our proposed wearable configuration significantly reduces the relative angular velocity between the robot and the subject regardless of the controller and walking speed, Figs. 8 and 10. This conclusion complements the theoretical results obtained previously, which showed reduced contact forces for the proposed configuration, which would also result in enhanced comfort. Our wearable configuration not only reduced wobbling, but also enhanced the metabolic reduction achieved with the exoskeleton across all participants (Table III) and regardless of which controller was used: Fig. 12(a) shows how the multi-strap configuration achieved a considerable metabolic reduction with the RL-based controller when compared with the same controller while wearing the single-strap configuration (18% reduction versus 6.3% increase). Participant 1, for instance, saw a 32.3% increase in metabolic cost at the tested speed even with the RL-based controller when wearing the single-strap configuration, but resulted in an 11.17% reduction when using the multi-strap configuration. Likewise, Fig. 12(b) shows that the RL controller reduces the metabolic cost of walking at the tested speed more than the gait-based controller, although the impact of the wearable configuration was more pronounced than the effect of the controller (Fig. 12(a) versus Fig. 12(b)). These results highlight the importance of a good wearable interface: a traditional, single-strap configuration widely used in state-of-the-art devices may translate into worse results than the same controller could achieve if supported by a more stable, comfortable wearable interface.

VII. CONCLUSION

This paper proposed a novel mechatronic design for hip-assistance exoskeletons, addressing key challenges in the current state-of-the-art. By maintaining torque density, backdrivability,

and high torque tracking performance thanks to the proposed QDD actuation, a novel wearable design paradigm is proposed. The design is supported by a multibody model to predict human-exoskeleton interaction forces. Based on our model, a new, multi-strap, waist-only configuration was introduced. Then, reaction forces and torques during gait were characterized using publicly available kinematic data from subjects walking overground. Following this design paradigm, we developed a new, user-centered hip exoskeleton with greater comfort. Experimental validation of the actuation units via torque tracking performance tests, as well as comfort metrics including a reduction in metabolic cost, wobbling, and a SUS survey, were analyzed. Experimental results prove the importance and impact of comfort-centered features upon the user experience: our wearable configuration significantly reduced wobbling (up to an average of 74%) compared to a traditional single-strap configuration and greatly benefits the metabolic cost reduction during ground-level walking. With a 9 Nm assistance, our user-centered exoskeleton achieved an average 18% reduction in the metabolic cost of walking with our proposed configuration and the reinforcement learning controller. In addition, our wearable configuration was also tested at a higher speed of 1.2 m/s, still resulting in a considerable reduction of wobbling versus the single-strap configuration. Furthermore, the effect of two controllers on the same metrics was also independently analyzed, it is more subtle in wobbling but significant in metabolic rate reduction. Our results lead to a portable, comfort-centered design for hip exoskeletons that improves the current state of the art. A more detailed analysis of physiological parameters, such as muscle activations or possible reductions in muscle fatigue, remains to be approached to further understand the beneficial effects of our design. Human-robot interaction is complex and encompasses many variables: experimental analysis of contact forces between the subject and the wearable interface may draw attention to variables not considered in this work, such as time-dependent variations in the wearable interface, which may appear in high wobbling conditions. Higher walking speeds may also be considered for different applications, and separate subjective questionnaires may be presented to participants per task and condition, providing insights on the subjective perception of each of them. A demonstration video of our current design can be found at https://youtu.be/V76xtamY-L4.

REFERENCES

[1] A. T. Asbeck, K. Schmidt, I. Galiana, D. Wagner, and C. J. Walsh, "Multi-joint soft exosuit for gait assistance," in *Proc. IEEE Int. Conf. Robot. Autom.*, 2015, pp. 6197–6204.

[2] Y. Lee et al., "Biomechanical design of a novel flexible exoskeleton for lower extremities," *IEEE/ASME Trans. Mechatronics*, vol. 22, no. 5, pp. 2058–2069, Oct. 2017.

[3] G. Lv, H. Zhu, and R. D. Gregg, "On the design and control of highly backdrivable lower-limb exoskeletons: A discussion of past and ongoing work," *IEEE Control Syst. Mag.*, vol. 38, no. 6, pp. 88–113, Dec. 2018.

[4] C. McGibbon et al., "Evaluation of a lower-extremity robotic exoskeleton for people with knee osteoarthritis," *Assist. Technol., Official J. RESNA*, vol. 34, pp. 543–556, Sep. 2022.

[5] J. Zhu, C. Jiao, I. Dominguez, S. Yu, and H. Su, "Design and backdrivability modeling of a portable high torque robotic knee prosthesis with intrinsic compliance for agile activities," *IEEE/ASME Trans. Mechatronics*, vol. 27, no. 4, pp. 1837–1845, Aug. 2022.

[6] J. Kim et al., "Reducing the metabolic rate of walking and running with a versatile, portable exosuit," *Science*, vol. 365, no. 6454, pp. 668–672, 2019.

[7] E. Martini et al., "Gait training using a robotic hip exoskeleton improves metabolic gait efficiency in the elderly," *Sci. Rep.*, vol. 9, no. 1, p. 7157, 2019.

[8] W. Cao, C. Chen, H. Hu, K. Fang, and X. Wu, "Effect of hip assistance modes on metabolic cost of walking with a soft exoskeleton," *IEEE Trans. Autom. Sci. Eng.*, vol. 18, no. 2, pp. 426–436, Apr. 2021.

[9] L. Chen, C. Chen, Z. Wang, X. Ye, Y. Liu, and X. Wu, "A novel lightweight wearable soft exosuit for reducing the metabolic rate and muscle fatigue," *Biosensors*, vol. 11, no. 7, p. 215, 2021.

[10] J. Kim et al., "Reducing the energy cost of walking with low assistance levels through optimized hip flexion assistance from a soft exosuit," *Sci. Rep.*, vol. 12, no. 1, 2022, Art. no. 11004.

[11] M. Sposito, S. Toxiri, D. G. Caldwell, J. Ortiz, and E. De Momi, "Towards design guidelines for physical interfaces on industrial exoskeletons: Overview on evaluation metrics," in *Wearable Robotics: Challenges and Trends*, M. C. Carrozza, S. Micera, and J. L. Pons, Eds., Cham, Switzerland: Springer, 2019, pp. 170–174. [Online]. Available: https://link.springer.com/chapter/10.1007/978-3-030-01887-0_33

[12] M. B. Yandell, B. T. Quinlivan, D. Popov, C. Walsh, and K. E. Zelik, "Physical interface dynamics alter how robotic exosuits augment human movement: Implications for optimizing wearable assistive devices," *J. Neuroeng. Rehabil.*, vol. 14, no. 1, p. 40, 2017.

[13] J. Wolff, C. Parker, J. Borisoff, W. B. Mortenson, and J. Mattie, "A survey of stakeholder perspectives on exoskeleton technology," *J. Neuroeng. Rehabil.*, vol. 11, no. 1, p. 169, 2014.

[14] R. Hybart, K. S. Villancio-Wolter, and D. P. Ferris, "Metabolic cost of walking with electromechanical ankle exoskeletons under proportional myoelectric control on a treadmill and outdoors," *PeerJ*, vol. 11, Jul. 2023, Art. no. e15775.

[15] P. Slade, M. J. Kochenderfer, S. L. Delp, and S. H. Collins, "Personalizing exoskeleton assistance while walking in the real world," *Nature*, vol. 610, no. 7931, pp. 277–282, 2022.

[16] L. M. Mooney and H. M. Herr, "Biomechanical walking mechanisms underlying the metabolic reduction caused by an autonomous exoskeleton," *J. Neuroeng. Rehabil.*, vol. 13, no. 1, p. 4, 2016.

[17] C. Buesing et al., "Effects of a wearable exoskeleton stride management assist system (SMA®) on spatiotemporal gait characteristics in individuals after stroke: A randomized controlled trial," *J. Neuroeng. Rehabil.*, vol. 12, no. 1, p. 69, 2015.

[18] B. Aakash et al., "Design and validation of a versatile high torque quasidirect drive hip exoskeleton," *IEEE/ASME Trans. Mechatronics*, vol. 29, no. 1, pp. 789–797, Feb. 2024.

[19] R. L. Medrano, G. C. Thomas, and E. J. Rouse, "Can humans perceive the metabolic benefit provided by augmentative exoskeletons?" *J. Neuroeng. Rehabil.*, vol. 19, p. 26, Feb. 2022.

[20] A. Jayaraman et al., "Stride management assist exoskeleton vs functional gait training in stroke: A randomized trial," *Neurology*, vol. 92, pp. e263–e273, Jan. 2019.

[21] M. B. Yandell, D. M. Ziemnicki, K. A. McDonald, and K. E. Zelik, "Characterizing the comfort limits of forces applied to the shoulders, thigh and shank to inform exosuit design," *PloS ONE*, vol. 15, Feb. 2020, Art. no. e0228536.

[22] B. Quinlivan, A. Asbeck, D. Wagner, T. Ranzani, S. Russo, and C. Walsh, "Force transfer characterization of a soft exosuit for gait assistance," in *Proc. Int. Design Eng. Tech. Conf. Comput. Inf. Eng. Conf.*, Aug. 2015, pp. 1–8.

[23] J. T. Meyer, S. O. Schrade, O. Lambercy, and R. Gassert, "User-centered design and evaluation of physical interfaces for an exoskeleton for paraplegic users," in *Proc. IEEE Int. Conf. Rehabil. Robot.*, Jun. 2019, pp. 1159–1166.

[24] L. Chen, D. Zhou, and Y. Leng, "A systematic review on rigid exoskeleton robot design for wearing comfort: Joint self-alignment, attachment interface, and structure customization," *IEEE Trans. Neural Syst. Rehabil. Eng.*, vol. 32, pp. 3815–3827, 2024.

[25] W. Liu and B. M. Nigg, "A mechanical model to determine the influence of masses and mass distribution on the impact force during running," *J. Biomech.*, vol. 33, no. 2, pp. 219–224, 2000.

[26] Y. Lee et al., "A flexible exoskeleton for hip assistance," in *Proc. IEEE/RSJ Int. Conf. Intell. Robots Syst. (IROS)*, 2017, pp. 1058–1063.

[27] M. K. Ishmael, D. Archangeli, and T. Lenzi, "A powered hip exoskeleton with high torque density for walking, running, and stair ascent," *IEEE/ASME Trans. Mechatronics*, vol. 27, no. 6, pp. 4561–4572, Dec. 2022.

[28] S. W. John, K. Murakami, M. Komatsu, and S. Adachi, "Cross-wire assist suit concept, for mobile and lightweight multiple degree of freedom hip assistance," in *Proc. Int. Conf. Rehabil. Robot. (ICORR)*, 2017, pp. 387–393.

[29] F. Giovacchini et al., "A light-weight active orthosis for hip movement assistance," *Robot. Autonom. Syst.*, vol. 73, pp. 123–134, Nov. 2015.

[30] D. Zanotto, Y. Akiyama, P. Stegall, and S. K. Agrawal, "Knee joint misalignment in exoskeletons for the lower extremities: Effects on user's gait," *IEEE Trans. Robot.*, vol. 31, no. 4, pp. 978–987, Aug. 2015.

[31] S. Yu et al., "Quasi-direct drive actuation for a lightweight hip exoskeleton with high backdrivability and high bandwidth," *IEEE/ASME Trans. Mechatronics*, vol. 25, no. 4, pp. 1794–1802, Aug. 2020.

[32] S. Luo, G. Androwis, S. Adamovich, E. Nunez, H. Su, and X. Zhou, "Robust walking control of a lower limb rehabilitation exoskeleton coupled with a musculoskeletal model via deep reinforcement learning," *J. Neuroeng. Rehabil.*, vol. 20, no. 1, p. 34, 2023.

[33] C. L. Lewis and D. P. Ferris, "Invariant hip moment pattern while walking with a robotic hip exoskeleton," *J. Biomech.*, vol. 44, no. 5, pp. 789–793, 2011.

[34] A. T. Asbeck, K. Schmidt, and C. J. Walsh, "Soft exosuit for hip assistance," *Robot. Auton. Syst.*, vol. 73, pp. 102–110, Nov. 2015.

[35] A. R. Manzoori, D. Malatesta, J. Primavesi, A. Ijspeert, and M. Bouri, "Evaluation of controllers for augmentative hip exoskeletons and their effects on metabolic cost of walking: Explicit versus implicit synchronization," *Front. Bioeng. Biotechnol.*, vol. 12, Mar. 2024, Art. no. 1324587.

[36] N. Ratnakumar and X. Zhou, "Optimized torque assistance during walking with an idealized hip exoskeleton," in *Proc. Int. Design Eng. Techn. Conf. Comput. Inf. Eng. Conf.*, 2021, Art. no. V002T02A009.

[37] Y. Ding, M. Kim, S. Kuindersma, and C. J. Walsh, "Human-in-the-loop optimization of hip assistance with a soft exosuit during walking," *Sci. Robot.*, vol. 3, no. 15, 2018, Art. no. eaar5438.

[38] J. Kim, M. Raitor, C. K. Liu, and S. H. Collins, "Frontal hip exoskeleton assistance does not appear promising for reducing the metabolic cost of walking: A preliminary experimental study," bioRxiv, Preprint, 2023. [Online]. Available: https://doi.org/10.1101/2023.08.22.554212

[39] J. Park et al., "Effect of hip abduction assistance on metabolic cost and balance during human walking," *Sci. Robot.*, vol. 8, no. 83, 2023, Art. no. eade0876.

[40] M. A. Normand, J. Lee, H. Su, and J. S. Sulzer, "The effect of hip exoskeleton weight on kinematics, kinetics, and electromyography during human walking," *J. Biomechan.*, vol. 152, May 2023, Art. no. 111552.

[41] B. Li et al., "Biomechanical design analysis and experiments evaluation of a passive knee-assisting exoskeleton for weight-climbing," *Ind. Robot, Int. J.*, vol. 45, no. 4, pp. 436–445, Jan. 2019.

[42] T. Zhang, C. Ning, Y. Li, and M. Wang, "Design and validation of a lightweight hip exoskeleton driven by series elastic actuator with two-motor variable speed transmission," *IEEE Trans. Neural Syst. Rehabil. Eng.*, vol. 30, pp. 2456–2466, 2022.

[43] A. J. Young, J. Foss, H. Gannon, and D. P. Ferris, "Influence of power delivery timing on the energetics and biomechanics of humans wearing a hip exoskeleton," *Front. Bioeng. Biotechnol.*, vol. 5, p. 4, Mar. 2017.

[44] A. Di Lallo, S. Yu, J. E. Slightam, G. X. Gu, J. Yin, and H. Su, "Untethered fluidic engine for high-force soft wearable robots," *Adv. Intell. Syst.*, vol. 6, no. 11, 2024, Art. no. 2400171.

[45] S. Chen et al., "Wearable knee assistive devices for kneeling tasks in construction," *IEEE/ASME Trans. Mechatronics*, vol. 26, no. 4, pp. 1989–1996, Aug. 2021.

[46] N. Kau, A. Schultz, N. Ferrante, and P. Slade, "Stanford doggo: An open-source, quasi-direct-drive quadruped," in *Proc. Int. Conf. Robot. Autom. (ICRA)*, 2019, pp. 6309–6315.

[47] T.-H. Huang et al., "Modeling and stiffness-based continuous torque control of lightweight quasi-direct-drive knee exoskeletons for versatile walking assistance," *IEEE Trans. Robot.*, vol. 38, no. 3, pp. 1442–1459, Jun. 2022.

[48] C. A. Fukuchi, R. K. Fukuchi, and M. Duarte, "A public dataset of overground and treadmill walking kinematics and kinetics in healthy individuals," *PeerJ*, vol. 6, Apr. 2018, Art. no. e4640.

[49] S. L. Delp, J. P. Loan, M. G. Hoy, F. E. Zajac, E. L. Topp, and J. M. Rosen, "An interactive graphics-based model of the lower extremity to study orthopaedic surgical procedures," *IEEE Trans. Bio-Med. Eng.*, vol. 37, no. 8, pp. 757–767, Aug. 1990.

[50] S. Luo et al., "Experiment-free exoskeleton assistance via learning in simulation," *Nature*, vol. 630, no. 8016, pp. 353–359, 2024.

[51] P. W. Jordan, B. Thomas, I. L. McClelland, and B. Weerdmeester, *Usability Evaluation in Industry*. Boca Raton, FL, USA: CRC Press, 1996.

[52] J. Sauro, *A Practical Guide to the System Usability Scale: Background, Benchmarks & Best Practices*. Denver, CO, USA: Meas. Usabil. LLC, 2011.

[53] A. W. Heinemann, R. K. Bode, and C. O'Reilly, "Development and measurement properties of the orthotics and prosthetics users' survey (OPUS): A comprehensive set of clinical outcome instruments," *Prosthet. Orthot. Int.*, vol. 27, pp. 191–206, Dec. 2003.